Journal of Controlled Release 288 (2018) 227–238

Contents lists available at ScienceDirect

Journal of Controlled Release

journal homepage: www.elsevier.com/locate/jconrel

Therapeutic inhibition of spleen tyrosine kinase in inflammatory macrophages using PLGA nanoparticles for the treatment of non-alcoholic steatohepatitis

Dhadhang Wahyu Kurniawan[a,b], Arun Kumar Jajoriya[c], Garima Dhawan[c], Divya Mishra[c], Josepmaria Argemi[d], Ramon Bataller[d], Gert Storm[a,e], Durga Prasad Mishra[c], Jai Prakash[a,1], Ruchi Bansal[a,f,*,1]

[a] Department of Biomaterials Science and Technology, Technical Medical Centre, Faculty of Science and Technology, University of Twente, Enschede, the Netherlands
[b] Department of Pharmacy, Universitas Jenderal Soedirman, Indonesia
[c] Cell Death Research Laboratory, Division of Endocrinology, CSIR-Central Drug Research Institute, Lucknow, India
[d] Division of Gastroenterology, Hepatology and Nutrition, Pittsburgh Liver Research Center, University of Pittsburgh Medical Center, Pittsburgh, PA, USA
[e] Department of Pharmaceutics, Utrecht University, Utrecht, the Netherlands
[f] Department of Pharmacokinetics, Toxicology and Targeting, Groningen Research Institute of Pharmacy, University of Groningen, the Netherlands

ARTICLE INFO

Keywords:
Spleen tyrosine kinases SYK
Inflammatory Macrophages
Non-alcoholic steatohepatitis
PLGA nanoparticles
Targeted therapy
Inflammation

ABSTRACT

Non-alcoholic steatohepatitis (NASH) is the leading cause of cirrhosis worldwide and the most rapidly growing indication for liver transplantation. Macrophages are the important cellular component in the inflammatory milieu in NASH. Inflammatory and pro-fibrotic mediators produced by macrophages causes significant tissue injury in many inflammatory diseases. Therefore, inhibition of the inflammatory macrophages would be a promising approach to attenuate NASH. In this study, we studied the implication of SYK pathway in NASH, and investigated PLGA nanoparticles-based delivery of SYK pathway inhibitor as an effective and promising therapeutic approach for the treatment of NASH. We found positive correlation between SYK expression with the pathogenesis of NASH and alcoholic hepatitis in patients. Importantly, SYK expression was significantly induced in M1-differentiated inflammatory macrophages. To inhibit SYK pathway specifically, we used a small-molecule inhibitor R406 that blocks Fc-receptor signaling pathway and reduces immune complex-mediated inflammation. R406 dose-dependently inhibited nitric-oxide release and M1-specific markers in M1-differentiated macrophages. Thereafter, we synthesized PLGA nanoparticles to deliver R406 to increase the drug pharmacokinetics for the efficient treatment of NASH. We investigated the therapeutic efficacy of R406-PLGA in-vitro in differentiated macrophages, and in-vivo in Methionine-Choline-deficient (MCD)-diet induced NASH mouse model. R406-PLGA inhibited M1-specific differentiation markers in RAW and bone-marrow-derived macrophages. In-vivo, R406 and more strongly R406-PLGA ameliorated fibrosis, inflammation and steatosis in mice. R406 and more significantly R406-PLGA reduced ALT, AST, cholesterol and triglyceride plasma levels. These results suggest that delivery of SYK inhibitor using PLGA nanoparticles can be a potential therapeutic approach for the treatment of Non-alcoholic steatohepatitis.

1. Introduction

Cirrhosis and hepatocellular carcinoma (HCC) are the most common liver-related causes of morbidity associated with NASH (Non-alcoholic steatohepatitis) [1]. In the United States, NASH has already become the second-leading etiology of liver disease requiring liver transplantation in adults [2–4]. Advanced fibrosis or cirrhosis has been identified as the most important histological feature associated with NASH [5]. Liver fibrosis is the condition characterized by excessive accumulation of abnormal extracellular matrix (ECM) proteins, which results from chronic non-resolving inflammation [6,7]. The inflammation triggers the tissue destruction which further leads to scar tissue formation. Cell death and inflammation represent two characteristic but intricately linked features of the chronic liver disease that promote the

* Corresponding author at: Department of Biomaterials Science and Technology, University of Twente, Zuidhorst 245, Enschede 7500 AE, the Netherlands.
E-mail address: r.bansal@utwente.nl (R. Bansal).
[1] These authors contributed equally to this work.

https://doi.org/10.1016/j.jconrel.2018.09.004
Received 7 June 2018; Received in revised form 28 August 2018; Accepted 9 September 2018
Available online 13 September 2018

development of fibrosis [6,7].

Hepatic injury initiates a cascade of a fibrogenic process initiated by inflammatory and fibrogenic signals. The activation process is initiated by the release of growth factors, profibrogenic cytokines and chemokines by the injured hepatocytes, and inflammatory cells particularly macrophages and other non-parenchymal cells [6–8]. Hepatic macrophages arise from circulating bone-marrow-derived monocytes, which are recruited to the injured liver or from proliferating resident macrophages (Kupffer cells). Resident macrophages have shown to play a significant role in initiaton of the inflammatory responses during tissue injury, while infiltrating monocyte-derived macrophages leads to chronic liver inflammation and fibrogenesis [7]. During enhanced recruitment owing to liver damage and environmental cues, infiltrating monocytes undergo differentiation into two broad subsets of macrophages that are categorized as classically-activated (M1) or alternatively-activated (M2). The initial inflammatory response is predominantly mediated by classically-activated (M1-differentiated) macrophages (activated by Th1 cytokines e.g. IFN-γ and LPS). In contrast, the resolution phase of inflammation is driven by alternatively-activated (M2-differentiated) macrophages, stimulated by Th2 cytokines (IL-4 or IL-13) [7].

We have earlier demonstrated crucial role of signaling pathways in liver fibrogenesis [9–11]. Another major signaling pathway involved in the pathogenesis of liver disease is Spleen tyrosine kinase (SYK) signaling pathway [12–15]. SYK is a cytoplasmic tyrosine kinase of 72 KDa that belongs to ZAP70/SYK family of the non-receptor protein tyrosine kinases (PTKs) [16]. SYK was identified and known to be expressed in hematopoietic cells, including macrophages, and has shown to be important in the downstream signaling events that drive inflammatory pathways of both the innate and adaptive immune systems [16]. While most studies focused on hematopoietic cells, SYK has also been shown to be expressed in non-hematopoietic cells including fibroblasts and hepatocytes [15,17]. A recent study has reported the up-regulation of SYK in hepatocytes and activated HSCs during liver fibrosis that promotes HSCs activation and proliferation via crosstalk between cytokines secreted by hepatocytes and HSCs [15]. Many studies have also demonstrated the role of SYK in various inflammatory and fibrotic diseases, such as Rheumatoid Arthritis [18,19], allergic asthma/rhinitis [20,21], renal interstitial fibrosis [22] and that SYK inhibition could be a therapeutic strategy for the treatment of inflammation- and fibrosis-related diseases [15,16,18,20,22]. SYK functions via an immuno-receptor tyrosine-based activation motif (ITAM) or Toll-like receptors (TLRs) which are activated by pathogen-associated molecular patterns (PAMP) [16,23]. Selective SYK inhibition or deletion in macrophages has shown to reduce macrophage activation as shown by reduced production of FcγR (Fc gamma receptor), CCL2 (or MCP1, macrophage chemotactic protein 1), IL-6 and TNF-α (Tumor necrosis factor alpha) [16,23]. Therapeutic inhibition of SYK has shown to ameliorate inflammation and steatosis in Alcoholic liver diseases [12,13], and suppressed liver fibrosis via inhibition of HSC activation in animal models [15]. However, implication and inhibition of SYK pathway in NASH and specifically in M1 inflammatory macrophages has not been investigated yet.

Macrophages and especially the liver-resident Kupffer cells are in the focus of nanomedicine due to their highly efficient and non-specific uptake of many nanomaterials as well as due to their critical pathogenic functions during inflammation and fibrogenesis [24]. One of the nanoparticles is Poly(lactic-*co*-glycolic acid) (PLGA)-based nanoparticles that are widely used as drug delivery carriers in various biomedical applications such as vaccination, cancer, inflammation, and other diseases [25,26]. PLGA is a FDA-approved biodegradable polymer with favorable mechanical properties, biodegradation kinetics, drug compatibility and biocompatibility since PLGA is biologically hydrolyzed to metabolite monomers, lactic acid and glycolic acid [25]. These two monomers are endogenously metabolized by the body via the Krebs cycle therefore no systemic toxicity is associated with the utilization of PLGA for drug delivery. PLGA-nanoparticles are internalized in cells partly through fluid-phase pinocytosis and through Clathrin-mediated endocytosis [27].

In this study, we have analyzed the SYK expression in NASH and alcoholic hepatitis (AH) patients. We have further examined the expression and activation of SYK signaling pathway in inflammatory macrophages. We thereafter, using small-molecule SYK inhibitor R406, studied the implication of therapeutic SYK inhibition in inflammatory macrophages. For the efficient delivery of SYK inhibitor R406 in vivo, we synthesized R406-encapsulated PLGA nanoparticles and investigated their therapeutic efficacy in vitro in M1-differentiated RAW macrophages and murine bone marrow derived macrophages, and in vivo in MCD diet-induced NASH mouse model.

2. Materials and methods

2.1. Cell lines

Murine RAW 264.7 macrophages were obtained from the American Type Culture Collection (ATCC, Manassas, VA, USA). RAW macrophages were cultured in Roswell Park Memorial Institute (RPMI) 1640 medium (Lonza, Verviers, Belgium) supplemented with 2 mM L-glutamine (Sigma, St. Louis, MO), 10% fetal bovine plasma (FBS, Lonza) and antibiotics (50 U/mL Penicillin and 50 μg/mL streptomycin, Sigma).

2.2. Bone marrow derived macrophages

Bone marrow-derived macrophage (BMDM) cultures were freshly isolated from C57BL/6 mice as described previously elsewhere [28]. Briefly, femurs and tibias were flushed with Dulbecco's modified Eagle's medium (DMEM) (Life Technologies, Carlsbad, CA, USA) with 10% FBS (Lonza) to collect bone marrow. Cells were then triturated 3–5 times through an 18-gauge needle and centrifuged at 1200 rpm for 5 min. After removing supernatant, RBCs were lysed with the lysis buffer and the remaining cells were washed in DMEM +10% FBS and plated at 1×10^6 cells/mL in DMEM supplemented with 1% penicillin/streptomycin, 1% HEPES, 0.001% β-mercaptoethanol, 10% FBS, and 20% supernatant from mouse 3T3 fibroblasts [obtained from ATCC and cultured in cultured in (DMEM) medium supplemented with 2 mM L-glutamine (Sigma), 10% FBS (Lonza) and antibiotics (Sigma)]. The fibroblasts conditioned medium is required to promote differentiation of bone marrow cells into macrophages (7–10 days). Media was changed on days 2, 4, and 6, and cells were re-plated on day 7 for performing experiments.

2.3. PLGA nanoparticles preparation

Poly (D,L-lactide-co-glycolide) (PLGA) nanoparticles were prepared by the emulsification solvent evaporation method as described earlier [29]. Briefly, the internal phase containing 100 μL ethyl acetate containing 2.5 mg PLGA [Poly (D,L-lactide-co-glycolide, with a co-monomer ratio of 50/50 (lactic/glycolic acid), Mw = 17,000, Corbion Purac, Gorinchem, The Netherlands] and 40 μg R406 (Mw = 628.63, Selleckchem, Boston, NY) was emulsified into an external aqueous phase of 100 μL of 2% Poly (vinyl-alcohol) (PVA, Sigma) (*w/v*), drop by drop under constant vortexing at maximum speed. The formed o/w microemulsion was subsequently sonicated for 2 min at 5% power output. The emulsion was transferred into 40 mL of 0.3% PVA (w/v) under magnetic stirring, and stirred overnight at room temperature to evaporate organic solvent ethyl acetate and to solidify the emulsified nanodroplets. The formed nanoparticles were isolated by centrifugation for 60 min at 16,000 rpm (rotor SS-34, Sorvall RC-5C Plus, Kendro Lab, USA) and the supernatant was discarded. The resulting nanoparticles were characterized for their average size and size distribution by dynamic light scattering (DLS) and zeta potential measurements using a Nano ZS Zetasizer (Malvern Instruments Ltd., Malvern, UK). R406-

PLGA nanoparticles were characterized using Scanning electron microscope (JEOL JSM-IT 100, Akishima, Japan) with a secondary electron detector and an acceleration voltage of 3–5 kV. The nanoparticle dispersions were freeze-dried before-hand and mounted on conductive carbon tape.

2.3.1. Determination of R406 encapsulation

R406 drug encapsulation (% DE) was done by developed HPLC method using UPLC (Thermoscientific™ Dionex™ Ultimate™ 3000 system). Briefly, 50 μL samples R406-PLGA in suspension were centrifuged using MicroCL 17 centrifuge (Thermoscientific) for 5 min at 13,300 rpm. Filtrates were discarded and the pellet was dissolved in DMSO and measured with UPLC at λ_{max} 261 nm (Fig. S1A). Different drug concentrations were used, and measured with UPLC and plotted as a standard curve (Fig. S1B) for determination of drug concentration.

2.3.2. In vitro drug release and uptake by RAW macrophages

To perform the drug release study of R406 and R406-PLGA, we plated the RAW cells (5×10^5 cells/well) in 12 well plates and cultured overnight. Then we added R406 and R406-PLGA in the cells. Furthermore, 100 μL of samples were collected and replaced by an equal volume of the medium at time intervals (0, 6, 12, 24, and 48 h). The amount of drug released into the medium was calculated according to a standard curve of R406 which is measured with UPLC. Each experiment was conducted as three independent experiment ($n = 3$). We also performed the drug release study of R406 and R406-PLGA without RAW cells, i.e. in the complete medium for RAW cells. The drug and the nanoparticles with the medium incubated in a shaking incubator at 37 °C. The rest of the procedure was same as drug release study with RAW cells. The drug uptake was measured as % total drug (at different time points) - % total drug left in the medium (at different time points). The graphs were ploted as % cumulative drug release (to depict drug release) and % total drug uptake (to depict drug uptake by RAW macrophages).

2.4. In vitro efficacy studies in RAW cell macrophages

For differentiation of RAW macrophages, cells were plated (1×10^6 cells/well) in 12 well plates and cultured overnight. The cells were then incubated with LPS (100 ng/mL, Sigma) and IFNγ (10 ng/mL, Peprotech, Rocky Hill, NJ) for M1 differentiation, and IL-4 (10 ng/mL, Peprotech) and IL-13 (10 ng/mL, Peprotech) for M2 differentiation for 24 h. To study the effect of SYK inhibitor; RAW cells were incubated with medium alone, 0.5, 1.0 and 5.0 μM of SYK inhibitor R406 (Selleckchem, Boston, NY) together with M1 differentiation stimulus for 48 h. For the effect of SYK inhibitor R406 loaded nanoparticles (R406-PLGA), M1-differentiated macrophages were incubated either with 5 μM R406, R406-PLGA (equivalent dose, 5 μM) or PLGA (empty nanoparticles, equimolar concentration as R406-PLGA) for 48 h. Cells were then lysed either with protein lysis buffer for western blot analysis or RNA lysis buffer for quantitative real-time PCR analysis. All the efficacy studies were performed at least 3 times independently.

2.5. In vitro efficacy studies in freshly isolated murine bone marrow derived macrophages

Bone marrow derived macrophages were plated at a density of 1×10^6/mL and differentiated into M1 macrophages using LPS (100 ng/mL; sigma) and IFNγ (10 ng/mL, Peprotech), or M2 macrophages using IL-4 (10 ng/mL, Peprotech) and IL-13 (10 ng/mL, Peprotech). For efficacy studies, cells were incubated with medium alone, SYK-loaded nanoparticles (R406-PLGA), empty nanoparticles (PLGA) and free drug (R406) together with M1 stimulus. After 48 h of incubation, cells were lysed for RNA isolation and real-time PCR analysis. Three independent experiments were performed.

2.6. Nitric oxide (NO) release bioassay

The effect of R406 on M1 macrophages was assessed by measuring the inhibition of nitric oxide (NO) release as described earlier [30], a stable NO metabolite produced by M1 macrophages. RAW cells (2×10^5 cells/200 μL/well) were seeded in 96-well plates, were cultured overnight and incubated with IFNγ (10 ng/mL, Peprotech) and LPS (100 ng/mL, Sigma) together with different concentrations of SYK inhibitor R406 (0, 0.5, 1.0, and 5.0 μM). After 48 h, 100 μL culture supernatant was added to 100 μL of Griess reagent (1% sulfanilamide (Sigma), 0.1% naphthyl ethylenediamine dihydrochloride (Sigma); 3% phosphoric acid (Sigma)) and the absorbance at 540 nm was measured with a microplate reader. NO release assays were performed in triplicates in three independent experiments.

2.7. Cell viability assay

To assess the effects on cell viability, cells were plated in 96 well plates, cultured overnight and incubated with different concentrations of R406 (0.1, 0.5, 1.0, and 5.0 uM) together with M1 stimulus (100 ng/mL LPS and 10 ng/mL IFNγ) for 48 h. To study the effects of R406-PLGA on cell viability, cells were incubated with R406-PLGA (equivalent dose, 5 μM), PLGA (empty nanoparticles, equimolar concentration as R406-PLGA) or free drug R406 (5 μM) together with M1 stimulus for 48 h. Cell viability assays were performed using Alamar Blue reagent (Invitrogen, Carlsbad, CA, USA) as per manufacturer's instructions. The results are represented as % cell viability normalized to untreated control cells (at 100%). All measurements were performed in triplicates in three independent experiments.

2.8. Methionine and choline-deficient (MCD) diet model

Animal studies were conducted in strict accordance with the guidelines and ethical regulations for the Care and Use of Laboratory Animals, CSIR-Central Drug Research Institute, India. The protocols were approved by the Institutional Animal Ethics Committee at the CSIR-Central Drug Research Institute, India. 8-week old male C57BL/6 mice (Jackson Laboratories, Bar Harbor, USA) were fed on MCD diet (C1070, Altromin GmbH, Lage, Germany) for 4 weeks while the controls received regular chow diet ($n = 4$) for 4 weeks. In this study, we used male mice since it has been shown that male mice develop more severe fatty liver disease as compared to female mice. Furthermore, male mice were shown to be more vulnerable to hepatic lipid accumulation while on MCD diet as compared to female mice. This study also suggested the reduction of fatty liver disease development in female mice due to the sex hormones e.g. estrogen [31]. MCD male mice were treated for two weeks intravenously (three times per week) with vehicle (PBS, $n = 5$), R406 (10 mg/kg, n = 5), R406-PLGA (equivalent dose of 10 mg/kg, n = 5) or PLGA (empty nanoparticles, equimolar concentrations as R406-PLGA, n = 5) while continuing MCD diet (Fig. S2) At the end of the experiment, mice were euthanised and the liver tissues and blood samples were collected for analysis. Alanine aminotransferase (ALT), aspartate aminotransferase (AST), total plasma cholesterol levels and plasma triglycerides levels were measured by standard automated laboratory methods.

2.9. RNA extraction, reverse transcription, quantitative real-time PCR

Total RNA from cells and liver tissues was isolated using GenElute Total RNA Miniprep Kit (Sigma) and SV total RNA isolation system (Promega Corporation, Madison, WI, USA), respectively, according to manufacturer's instructions. The RNA concentration was quantitated by a UV spectrophotometer (NanoDrop Technologies, Wilmington, DE). Total RNA (1 μg) was reverse-transcribed using iScript cDNA Synthesis Kit (Bio-Rad, Hercules, CA). All the primers were purchased from Sigma-Genoysis (Haverhill, UK). Real-time PCR was performed using

2× SensiMix SYBR and Fluorescein Kit (Bioline, QT615–05, Luckenwalde, Germany), 20 ng cDNA and pre-tested gene-specific primer sets. The cycling conditions for the BioRad CFX384 Real-Time PCR detection system were 95 °C for 10 min, 40 cycles of 95 °C/15 s, 72 °C/15 s, and 58 °C/15 s. Finally, cycle threshold (Ct) values were normalized to reference gene 18 s rRNA and fold changes in expression were calculated using the $2^{-\Delta\Delta Ct}$ method. All primers were purchased from Sigma-Genosys (Haverhill, UK). The primer sequences are given in Table S1.

2.10. Western blot analysis

Cells were lysed using 1× Cell Lysis Buffer containing 1× DTT reducing agent (Cell Signaling Technology, Leiden, the Netherlands) and homogenized using ultra-sonication on ice. The samples were boiled and subjected to SDS-PAGE with 10% Tris-glycine gels (Life Technologies) followed by protein transfer onto PVDF membrane. The membranes were developed according to the standard protocols using primary and secondary antibodies (as mentioned in Table S2). The bands were developed using ECL detection reagent (Perkin Elmer Inc., Walthan, MA) and photographed using FluorChem M Imaging System (ProteinSimple, Alpha Innotech, San Leandro CA). Intensity of individual bands were quantified using NIH ImageJ densitometry software (NIH, Bethesda, MD), and expressed as % relative to β –actin or SYK.

2.11. Histological stainings

2.11.1. Immunostainings

Liver tissues were harvested and transferred to Tissue-Tek OCT embedding medium (Sakura Finetek, Torrance, CA) and snap-frozen in 2-methyl butane chilled in a dry ice. Cryosections (6 μm) were cut using a Leica CM 3050 cryostat (Leica Microsystems, Nussloch, Germany). The sections were air-dried and fixed with acetone for 20 min. Tissue sections were rehydrated with PBS and incubated with the primary antibody for overnight at 4 °C. Sections then were incubated with horseradish peroxidase (HRP)-conjugated secondary antibody for 1 h at room temperature. Then incubated with HRP-conjugated tertiary antibody for 1 h at room temperature. Afterwards, peroxidase activity was developed using AEC (3-amino-9-ethyl carbazole) substrate kit (Life Technologies, Carlsbad, CA) for 20 min and nuclei were counterstained with hematoxylin (Fluka Chemie, Buchs, Switzerland). Endogenous peroxidase activity was blocked by 3% H_2O_2 prepared in methanol. The sections were mounted with Aquatex mounting medium (Merck, Darmstadt, Germany) and were scanned using Hamamatsu NanoZoomer Digital slide scanner 2.0HT (Hamamatsu Photonics, Bridgewater, NJ). The details about the antibodies used for immunostainings are provided in Table S2.

2.11.2. Oil-Red-O staining

Oil-Red-O stock solution was prepared by dissolving 0.3 g Oil-Red-O (Sigma) in 100 mL isopropanol. Sections were fixed in 4% formalin for 20 min and were then stained in Oil-Red-O solution as per manufacturer's instructions. Briefly, formalin-fixed sections were rinsed with 60% isopropanol followed by staining with freshly prepared Oil Red O working solution for 15 min. Thereafter, sections were rinsed with 60% isopropanol and nuclei were counterstained with hematoxylin (Fluka Chemie). Finally, sections were rinsed with tap water and were mounted with aquatex mounting medium (Merck).

2.11.3. Hematoxylin and Eosin staining

Sections were fixed with 4% formalin for 20 min and then rinsed with distilled water. The sections were incubated with hematoxylin for 15 min followed by washings with tap water. Thereafter, sections were incubated with eosin solution for 1.5 min followed by wash in 96% ethanol, dehydration with ethanol and were mounted with VectaMount mounting medium (Vector Laboratories, Burlingame, CA).

2.11.4. Quantitative histological analysis

For quantitation, stained sections were scanned at high resolution using Hamamatsu NanoZoomer Digital slide scanner 2.0HT (Hamamatsu Photonics). High resolution scans were viewed using NanoZoomer Digital Pathology (NDP2.0) viewer software (Hamamatsu Photonics). About 20 images (100×) of each entire section (from NDP) were imported into ImageJ software and were analyzed quantitatively at a fixed threshold.

2.12. SYK gene expression in the human liver tissues

SYK mRNA expression was assessed in the publicly available transcriptome datasets of liver tissue from patients with NASH (GSE48452) [32] obtained from the National Center for Biotechnology Information Gene Expression Omnibus database (GEO). Patients were categorized into 4 groups as per biopsy-based pathological investigation: control group ($n = 23$); NAFLD activity score NAS 1–2 ($n = 13$); NAS 3–4 ($n = 7$) and NAS 5–6 ($n = 15$).

High-throughput transcriptome profiling was performed using Illumina HiSeq2000 platform (San Diego, CA) with liver samples provided by the InTeam Consortium (Human Biorepository Core, University of Pittsburgh, PA) as described recently [18]. SYK mRNA expression was evaluated in patients with different phenotypes: 11 patients with non-severe alcoholic hepatitis (with Maddrey's discriminant function, MDF ≤32); AH responders (with severe alcoholic hepatitis (MDF > 32) patients responsive to steroids, $n = 9$) AH non-responders (AH severe alcoholic hepatitis (MDF > 32) patients non-responsive to steroids therapy, n = 9) and 10 patients with explants who underwent early liver transplantation for severe alcoholic hepatitis. Controls ($n = 10$) were non-diseased livers obtained from biopsied single nodules, whose histology was without significant alterations.

2.13. Statistical analyses

All the data are presented as a mean + standard error of the mean (SEM). The graphs and statistical analyses were performed using GraphPad Prism version 5.02 (GraphPad Prism Software, Inc., La Jolla, CA). Comparison to control group were analyzed using unpaired students' *t*-test while multiple comparisons between different groups were performed by one-way analysis of variance (ANOVA) with Bonferroni post-hoc test. The differences were considered significant at $p < .05$.

3. Results and discussion

3.1. Upregulation of SYK expression in NASH and AH patients, and inflammatory macrophages

Previous studies have documented that the functional inhibition of SYK pathway attenuates the severity of inflammatory diseases and fibrotic diseases [12,13,15,16]. In this study, we investigated the association of SYK expression with pathogenesis of NASH (non-alcoholic steatohepatitis) and AH (Alcoholic hepatitis). Using transcriptome analysis, we found a highly significant induction of SYK expression that correlated with the increasing NAS score (NAFLD activity score) as compared to normal livers (GEO accession number: GSE48452) (Fig. 1A). In AH patients, we found a significant correlation between AH severity and SYK expression (Fig. 1B) with increasing SYK expression from healthy individuals to AH non-severe, AH responders (AH patients responsive to steroids), AH non-responders (AH patients non-responsive to steroids therapy) and AH explants (AH severe patients with early liver transplantation). Likewise, previous studies have shown correlation of SYK and SYK pathway activation in liver fibrosis and alcoholic liver disease (ALD) patients as compared to healthy controls [13,15]. Since macrophages are the key pathogenic cells in NASH and

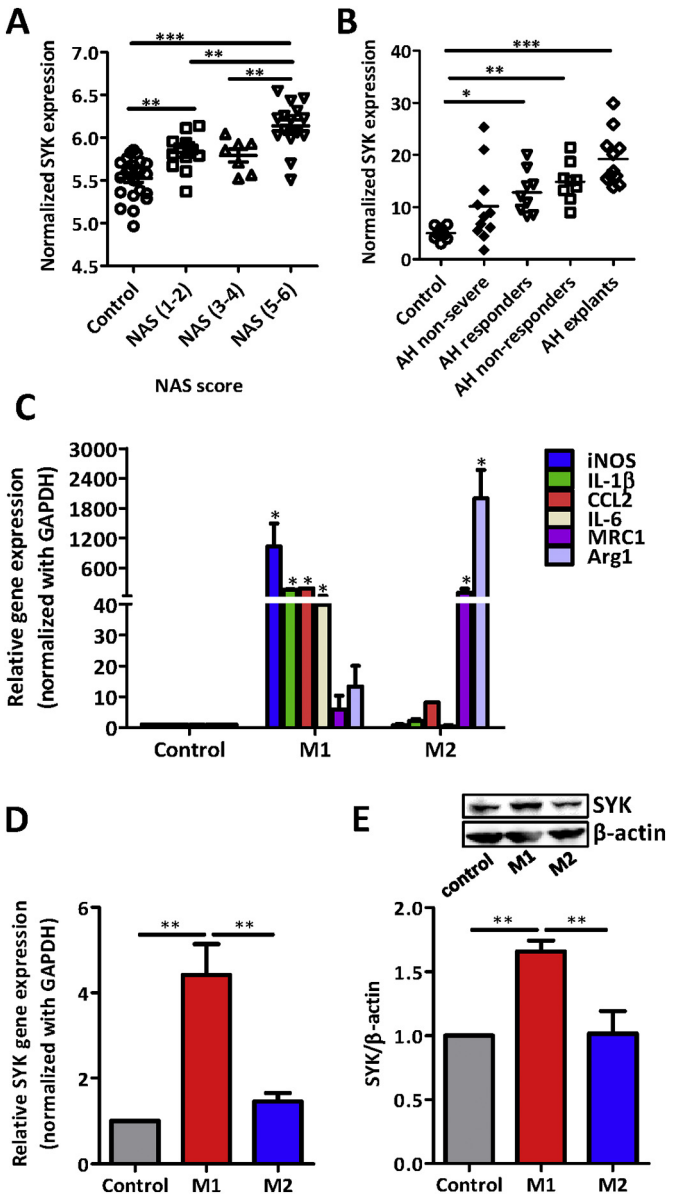

Fig. 1. Upregulation of SYK expression in NASH and AH patients, and differentiated macrophages. (A) Normalized SYK mRNA expression in the liver tissues from NASH patients: Control (n = 23); NAFLD activity score (NAS) 1–2 (n = 13); NAS 3–4 (n = 7); NAS 5–6 (n = 15). (B) Normalized SYK mRNA expression in the alcoholic hepatitis (AH) patients: controls (non-diseased livers, n = 10); AH non-severe (n = 11 patients); AH responders (AH patients responsive to steroids, n = 9); AH non-responders (AH patients non-responsive to steroids therapy, n = 9) and AH explants (AH severe patients with early liver transplantation, n = 11). (C) Gene expression of macrophage differentiation markers: iNOS, IL-1β, CCL2, IL-6 (M1 macrophages); MRC1 and ARG1 (M2 macrophages). Expression values for the respective genes in control M0 macrophages were set at 1.0 to calculate the relative gene expression in M1 and M2 macrophages. (D) SYK gene expression in the undifferentiated macrophage (control), M1 and M2 macrophages. (E) SYK protein expression as compared to β-actin and the respective quantitative analysis. Data are presented as mean ± SEM. *p < 0.05, **p < 0.01 and ***p < 0.001 denotes significance.

inflammatory liver diseases [33], we analyzed the SYK expression in differentiated murine RAW macrophages i.e. LPS- and IFNγ-induced M1-differentiated inflammatory macrophages, and IL-4- and IL-13-induced M2-differentiated restorative macrophages. We first confirmed the differentiation of macrophages using M1 and M2-specific markers and found that M1-differentiated macrophages significantly expressed M1 markers i.e. iNOS (inducible nitric oxide synthase or NOS2), IL-1β (Interleukin-1-beta), CCL2 [chemokine (C—C motif) ligand 2 or MCP1, monocyte chemoattractant protein 1] and IL-6 (Interleukin-6) while M2-differentiated macrophages expressed M2 markers i.e. MRC1 (mannose receptor complex 1) and ARG (Arginase I) (Fig. 1C). We then analyzed SYK expression in these differently differentiated macrophages. We observed significant upregulation of SYK mRNA and protein expression in LPS- and IFNγ-differentiated M1 inflammatory macrophages as compared to undifferentiated macrophages, and IL-4 and IL-13-mediated M2-differentiated restorative macrophages (Fig. 1D,E). These results suggest SYK as an appropriate molecular target in macrophages and inflammatory liver diseases especially NASH.

3.2. SYK inhibitor R406 inhibited LPS- and IFNγ-induced SYK activation in murine RAW macrophages

Since SYK expression was upregulated in M1-differentiated inflammatory macrophages, we explored the implication of this receptor in macrophages. We used R406 which is a potent SYK inhibitor (Fig. 2A), to inhibit SYK signaling pathway, that has been used earlier [13]. We first examined the phosphorylation of SYK and observed that increased SYK expression in M1 macrophages was accompanied with increased phosphorylation of SYK (Fig. 2B,C). We then tested the effect of R406 on SYK phosphorylation and functional activation i.e. nitric oxide (NO) release in M1-differentiated macrophages. We found that R406 concentration dependently reduced SYK phosphorylation i.e. SYK signaling pathway (Fig. 2B,C) and LPS- and IFNγ-induced NO release (Fig. 2D). In addition, we performed viability studies and found no toxicity with R406 (Fig. S3).

3.3. SYK inhibitor R406 inhibited gene expression of inflammatory markers in mouse RAW macrophages

We further examined the efficacy of R406 on gene expression of inflammatory markers in M1-differentiated macrophages. We observed that R406 concentration dependently inhibited LPS- and IFNγ-induced gene expression of M1 markers i.e. IL1β, Fc gamma receptor 1 (FcγR1), iNOS, CCL2 (or MCP1), IL-6 and CCR2 (C—C motif chemokine receptor 2) (Fig. 3A-F). These results are consistent with previous studies in experimental animal models [13,34,35]. Altogether, these results suggest that SYK inhibitor R406 treatment can potentially inhibit inflammatory macrophages and hence R406 has high potency for the treatment of inflammation-associated diseases. Inflammation in the liver protects this organ from infection and injury, but excessive inflammation may lead to extensive loss of hepatocytes, ischemia-reperfusion injury, metabolic alterations, and eventually hepatic damage. Therefore, inhibition of inflammation or inflammatory macrophages via SYK pathway inhibition might be promising approach for the treatment of inflammatory liver diseases.

3.4. Preparation and characterization of R406-PLGA nanoparticles

Since small-molecule tyrosine kinase inhibitors have been shown to have poor pharmacokinetics and bioavailability [36], we prepared R406-encapsulated PLGA nanoparticles (R406-PLGA, Fig. 4A) to improve the pharmacokinetics and thereof in vivo therapeutic efficacy of R406. R406-PLGA nanoparticles (R406-PLGA) were analyzed for the morphology, size and zeta potential (Fig. 4B,C). R406-PLGA has Z-average 159.7 nm, with almost comparable size to the control empty PLGA nanoparticles (PLGA) (Fig. 4C). The zeta potential was towards negative as shown in Fig. 4C. We also measured the drug encapsulation of R406 in the PLGA nanoparticles using HPLC (Fig. S1A,B). The drug encapsulation of R406 in the PLGA nanoparticles was found to be 37.49%. We further examined the physical stability of the R406-PLGA nanoparticles and observed that the particle size remained relatively stable at around 160 nm size after 46 days. These results suggest the

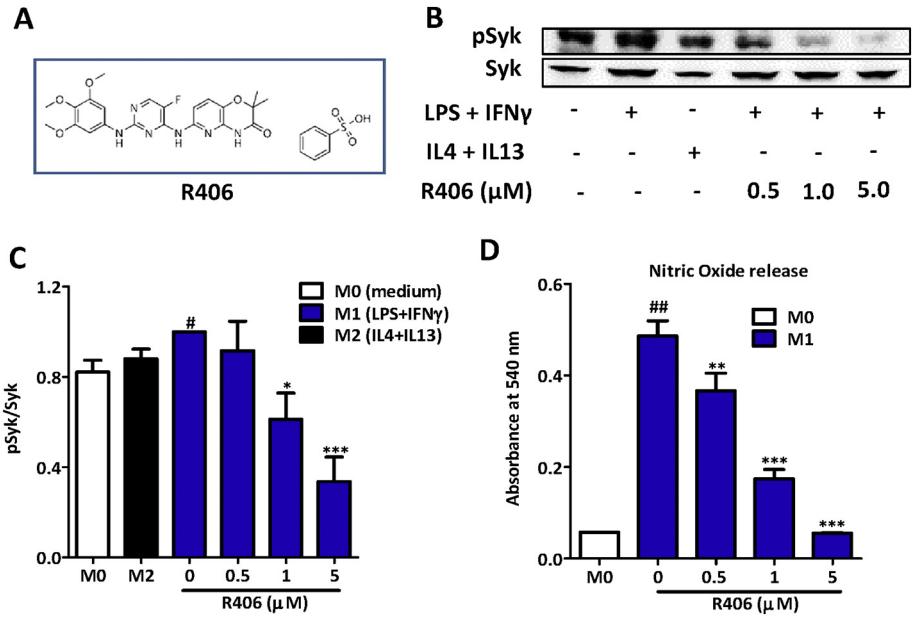

Fig. 2. Inhibition of SYK phosphorylation and nitric oxide release by SYK inhibitor R406 in RAW macrophages. (A) Structure of R406, a SYK inhibitor. (B) Protein expression and (C) quantitative densitometry analysis of phosphorylated SYK (pSYK) as compared to SYK in RAW 264.7 macrophages after incubation with medium alone, M2 stimulus (10 ng/mL IL-4 and 10 ng/mL IL-13) and M1 stimulus (100 ng/mL LPS + 10 ng/mL IFNγ) without and with R406 (0, 0.5, 1 and 5 μM). (D) Nitric oxide (NO) release as measured in the culture supernatant of RAW 264.7 cells incubated with medium alone (M0 or control) or M1 stimulus (100 ng/mL LPS + 10 ng/mL IFNγ) with R406 (0, 0.5, 1 and 5 μM). Data are presented as mean + SEM. #$p < 0.05$, ##$p < 0.01$ denotes significance versus control M0 undifferentiated macrophages. *$p < 0.05$, **$p < 0.01$ and ***$p < 0.001$ denotes significance versus M1-differentiated macrophages.

successful synthesis of R406-PLGA nanoparticles with favorable particle size and stability for appropriate delivery of SYK inhibitor.

3.5. R406-PLGA nanoparticles inhibited the SYK signaling pathway and gene expression of inflammatory markers in RAW macrophages

Following successful synthesis of R406-PLGA nanoparticles, we examined the R406 efficacy after encapsulation in PLGA nanoparticles.

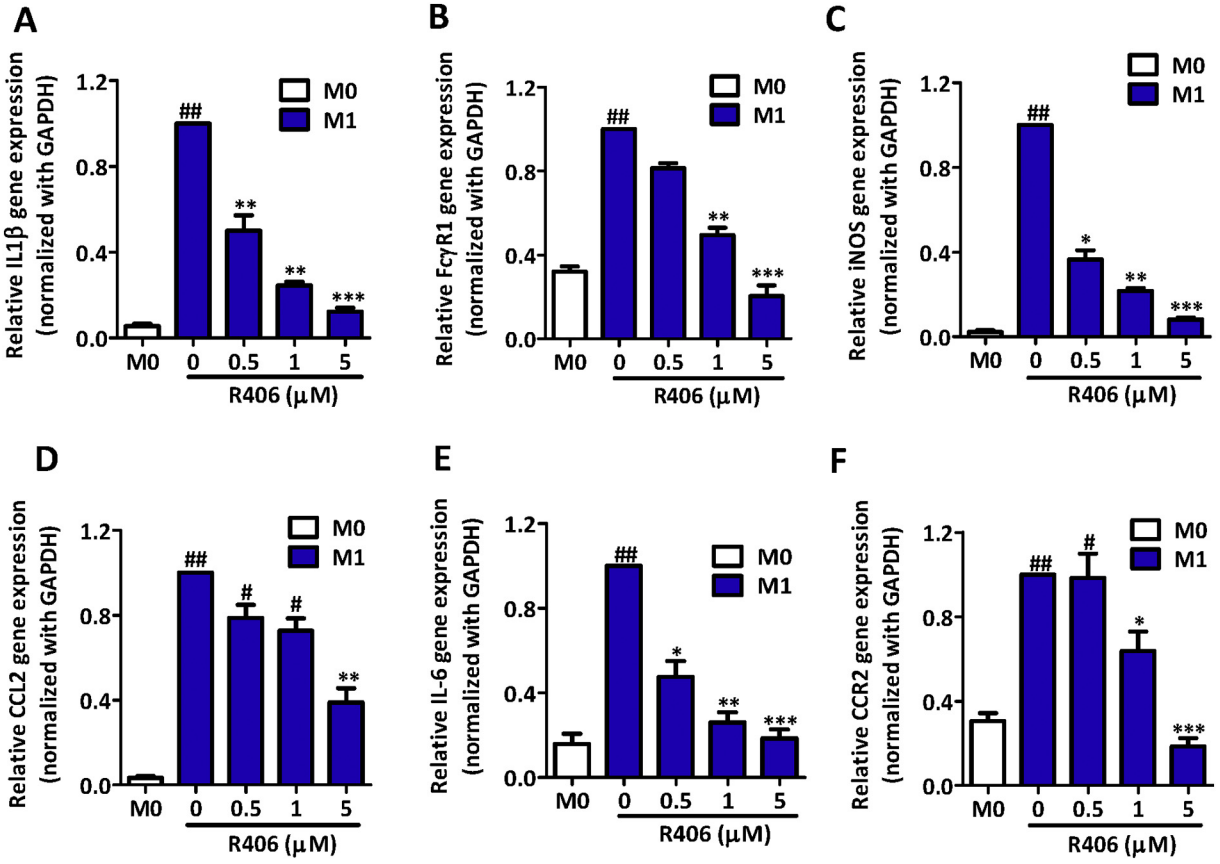

Fig. 3. Inhibition of M1-specific differentiation and inflammatory markers by R406 in RAW macrophages. Gene expression of M1 markers IL-1β (A); FcγR1 (B); iNOS (C); CCL2 (D); IL-6 (E); and CCR2 (F) in RAW 264.7 cells after incubation with medium alone (M0) or M1 stimulus with R406 (0, 0.5, 1, and 5 μM). Expression values for the respective genes in untreated M1 macrophages were set at 1.0 to calculate the relative gene expression. Data are presented as mean + SEM. #$p < 0.05$, ##$p < 0.01$ denotes significance versus control M0 macrophages.*$p < 0.05$, **$p < 0.01$ and ***$p < 0.001$ denotes significance versus M1-differentiated macrophages.

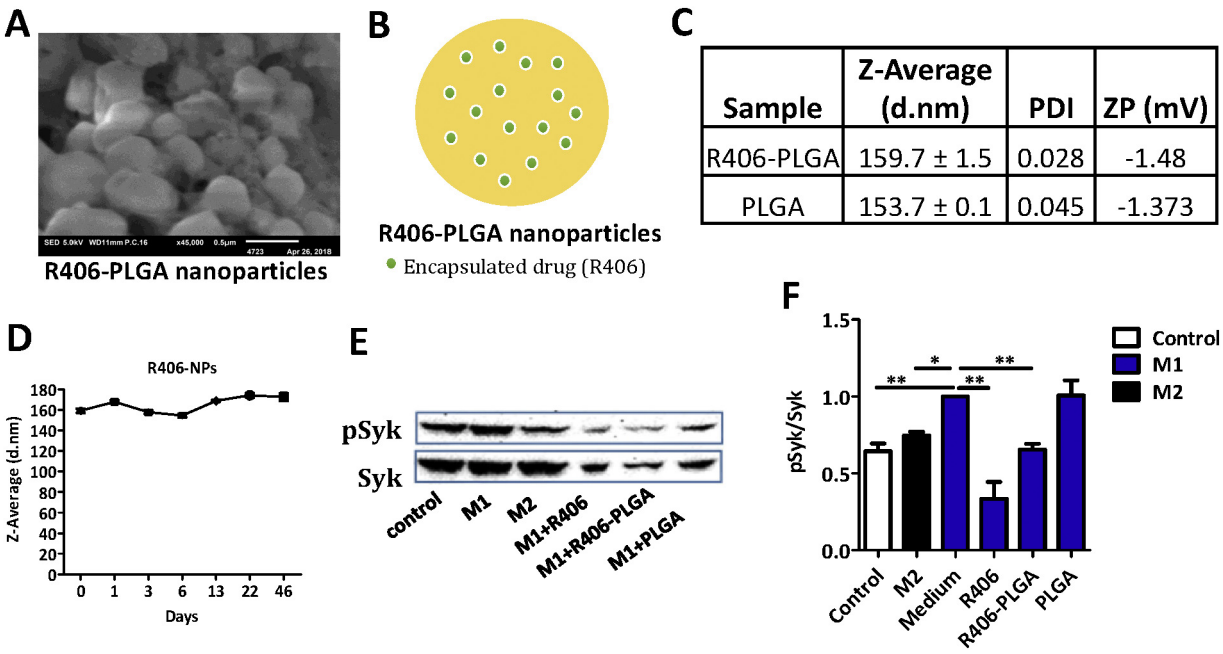

Fig. 4. Characterization of R406-PLGA nanoparticles: (A) Representative Image of R406-PLGA nanoparticles as characterized by scanning electron microscope (SEM); (B) Schematic representation depicting the drug (R406) encapsulated in the PLGA nanoparticles; (C) The average particle size, polydispersity index (PDI), and zeta potential (ZP) of R406-PLGA NPs (or R406-PLGA) as compared to empty-NPs (PLGA); (D) Physical stability (size stability) of R406-PLGA NPs for 46 days. (E) Protein expression and (F) quantitative densitometry analysis of pSYK compared to SYK on RAW 264.7 cells after incubation with medium alone (control), M2 stimulus (10 ng/mL IL-4 and 10 ng/mL IL-13), M1 stimulus (100 ng/mL LPS + 10 ng/mL IFNγ) with or without R406 (free drug), R406-PLGA or empty-NPs (PLGA). Data are presented as mean + SEM. *p < 0.05 and **p < 0.01 denotes significance.

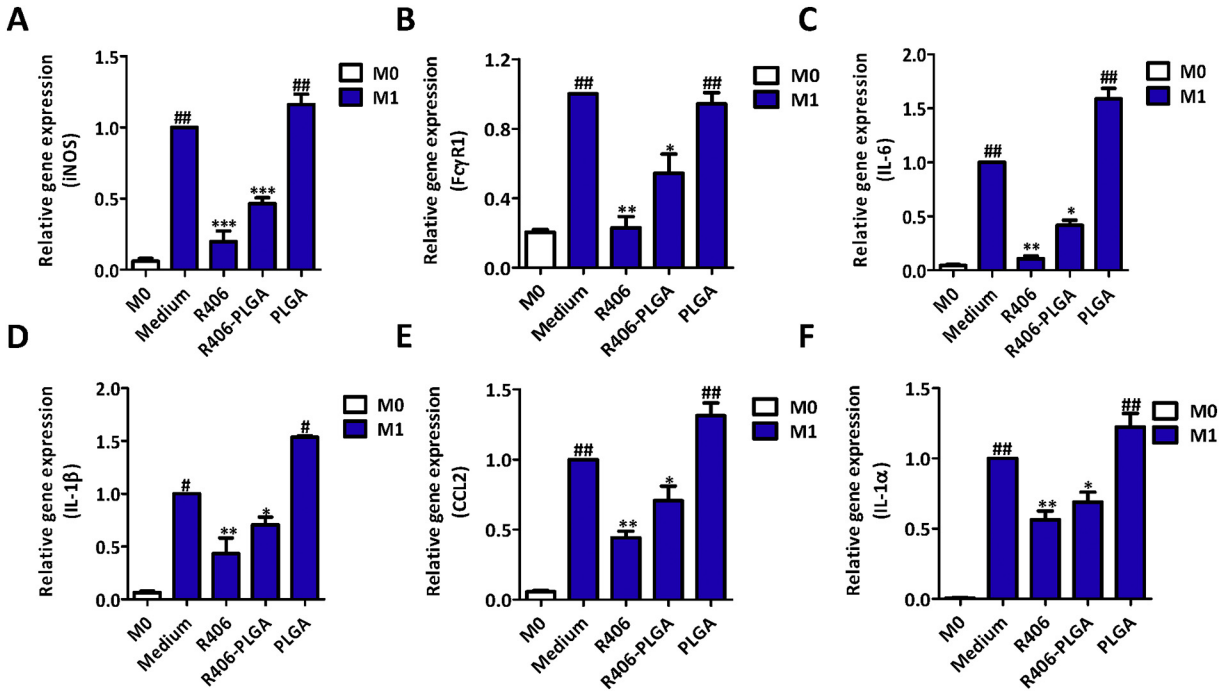

Fig. 5. Inhibition of inflammatory markers or M1 differentiation markers by R406 and R406-PLGA in RAW macrophages. Gene expression of inflammatory or M1-differentiation macrophages markers in RAW 264.7 cells: (A) iNOS; (B) FcγR1; (C) IL-6; (D) IL-1β; (E) CCL2 and (F) IL-1α after incubation with medium alone (M0 undifferentiated macrophages) or M1 stimulus (100 ng/mL LPS + 10 ng/mL IFNγ) with or without R406 (free drug), R406-PLGA or empty-NPs (PLGA). Data are presented as mean + SEM. #p < 0.05, ##p < 0.01 denotes significance versus control M0 macrophages. *p < 0.05, **p < 0.01 and ***p < 0.001 denotes significance versus M1-differentiated macrophages.

We first tested R406-PLGA nanoparticles in RAW macrophages for inhibition of SYK pathway and we found that both R406 and R406-PLGA nanoparticles significantly inhibited the SYK signaling pathway (SYK phosphorylation) as shown in Fig. 4E,F. While empty PLGA nanoparticles alone didn't show any effect in SYK phosphorylation (Fig. 4E,F). We further investigated the therapeutic effects of R406-PLGA nanoparticles in M1-differentiated inflammatory macrophages. Interestingly, both R406 and R406-PLGA nanoparticles significantly

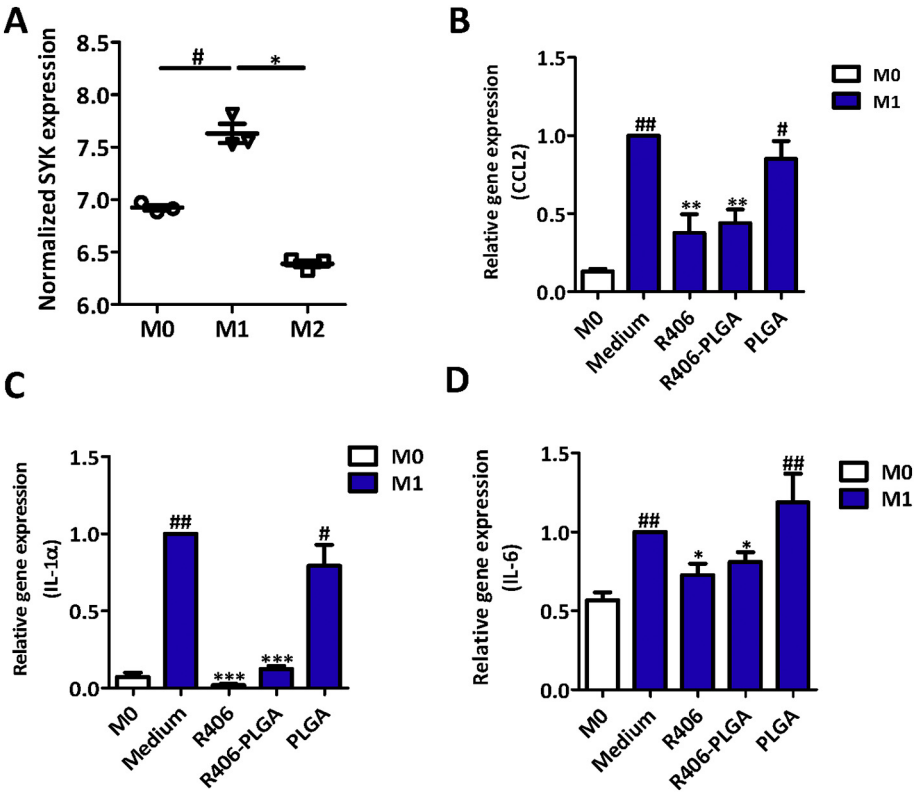

Fig. 6. Inhibition of inflammatory markers or M1 differentiation markers by R406 and R406-PLGA in murine bone marrow derived macrophages. (A) Normalized SYK expression in undifferentiated M0, M1-differentiated and M2-differentiated macrophages. Gene expression of inflammatory markers: (B) CCL2; (C) IL-1α and (D) IL-6 after incubation with medium alone (undifferentiated M0 macrophages) or M1 stimulus (100 ng/mL LPS + 10 ng/mL IFNγ) with or without R406 (free drug), R406-PLGA or empty-NPs (PLGA). Data are presented as mean + SEM. #$p < 0.05$, ##$p < 0.01$ denotes significance versus control M0 macrophages. *$p < 0.05$, **$p < 0.01$ and ***$p < 0.001$ denotes significance versus M1-differentiated macrophages.

inhibited the gene expression of M1-specific markers i.e. iNOS, FcγR1, IL-6, IL-1β, CCL2 and IL-1α (Fig. 5A-F). However, we observed R406 was more effective than R406-PLGA nanoparticles which is probably due to slow drug release kinetics of PLGA nanoparticles [25]. Generally, higher content of polyglycolide leads to quicker rates of degradation with an exception of 50:50 ratio of PLA/PGA which is used in this study exhibits the fastest degradation. As per modeling studies, PLA/PGA 50:50 demonstrated release kinetics of about 2–3 weeks to achieve 100% drug release [25]. Furthermore, studies have found, that the type of drug also plays a critical role in determining the release kinetics [37]. We performed drug release studies using R406-PLGA nanoparticles and found that % cumulative release of R406 from PLGA nanoparticles increases gradually after incubation for 48 h as compared to the free drug (Fig. S4A). Furthermore, we performed drug uptake studies and observed that R406 (in free form) was significantly taken up more in RAW macrophages (about 54% at 48 h) as compared to R406 (from PLGA nanoparticles) (about 45% at 48 h) as can be seen in Fig. S4B. These data supports the reduced in vitro therapeutic efficacy of R406-PLGA as compared to free R406, however further suggest slow and gradual release of R406 which will be desired in vivo. Essentially, these results also suggest that R406 retained its therapeutic effects following encapsulation in PLGA nanoparticles. We also performed the cell viability studies with R406-PLGA nanoparticles and observed no effect on cell viability as shown in Fig. S5.

3.6. R406-PLGA nanoparticles inhibited the SYK signaling pathway and gene expression of inflammatory markers in murine bone marrow derived macrophages

In general, immortalized cells are not considered normal as they divide indefinitely and express unique gene patterns that are not found in cell type in vivo and hence they might not have the relevant attributes of normal cells. Thus, it is important to validate the characteristics and results on primary cells that have not been passaged many times. To mimic the in vivo more closely, we performed studies on primary murine bone marrow derived macrophages (BMDMs). We first investigated the expression of SYK in BMDMs and observed significant upregulation of SYK expression in M1-differentiated BMDMs as compared to undifferentiated and M2-differentiated BMDMs (Fig. 6A). Thereafter, we examined the effect of R406-PLGA nanoparticles on the gene expression of inflammatory markers in M1-differentaited inflammatory BMDMs. We found that both R406 and R406-PLGA nanoparticles induced highly significant down-regulation in the expression levels of major inflammatory markers i.e. CCL2, IL-1α and IL-6 as shown in Fig. 6B-D. These results further confirmed our previous results in RAW macrophages and suggest that R406 retained its therapeutic efficacy after encapsulation in PLGA nanoparticles. Notably, we did not observe any effects from empty PLGA nanoparticles in RAW macrophages and in BMDMs (Fig. 5A-F, 6B-D).

3.7. R406-PLGA nanoparticles ameliorated liver inflammation, fibrosis and steatosis in MCD diet induced NASH mouse model

Finally, we investigated the therapeutic efficacy of R406-PLGA nanoparticles in MCD-diet induced NASH mouse model. We first examined the expression of SYK expression in mice with MCD-diet induced NASH and found that SYK expression was highly significantly induced in mice with NASH as compared to healthy controls. With this observation, we surmised that SYK play a major role in MCD-diet induced liver steatosis. We then examined the therapeutic efficacy of R406 and R406-PLGA nanoparticles in MCD-diet induced NASH. We followed the clinical treatment regimen, where we induced NASH for 4 weeks and treated mice for last 2 weeks with in total 4 intravenous administrations while continuing with MCD diet (Fig. S2). Morphological examination of liver tissues at the end of the study showed the visible pale and gross appearance suggesting the hepatocellular damage in MCD-diet induced NASH mice as compared to normal healthy control group (Fig. 7B). Treatment with R406 and R406-PLGA showed considerably better appearance of livers in contrast to MCD-diet induced NASH livers and PLGA-treated NASH livers

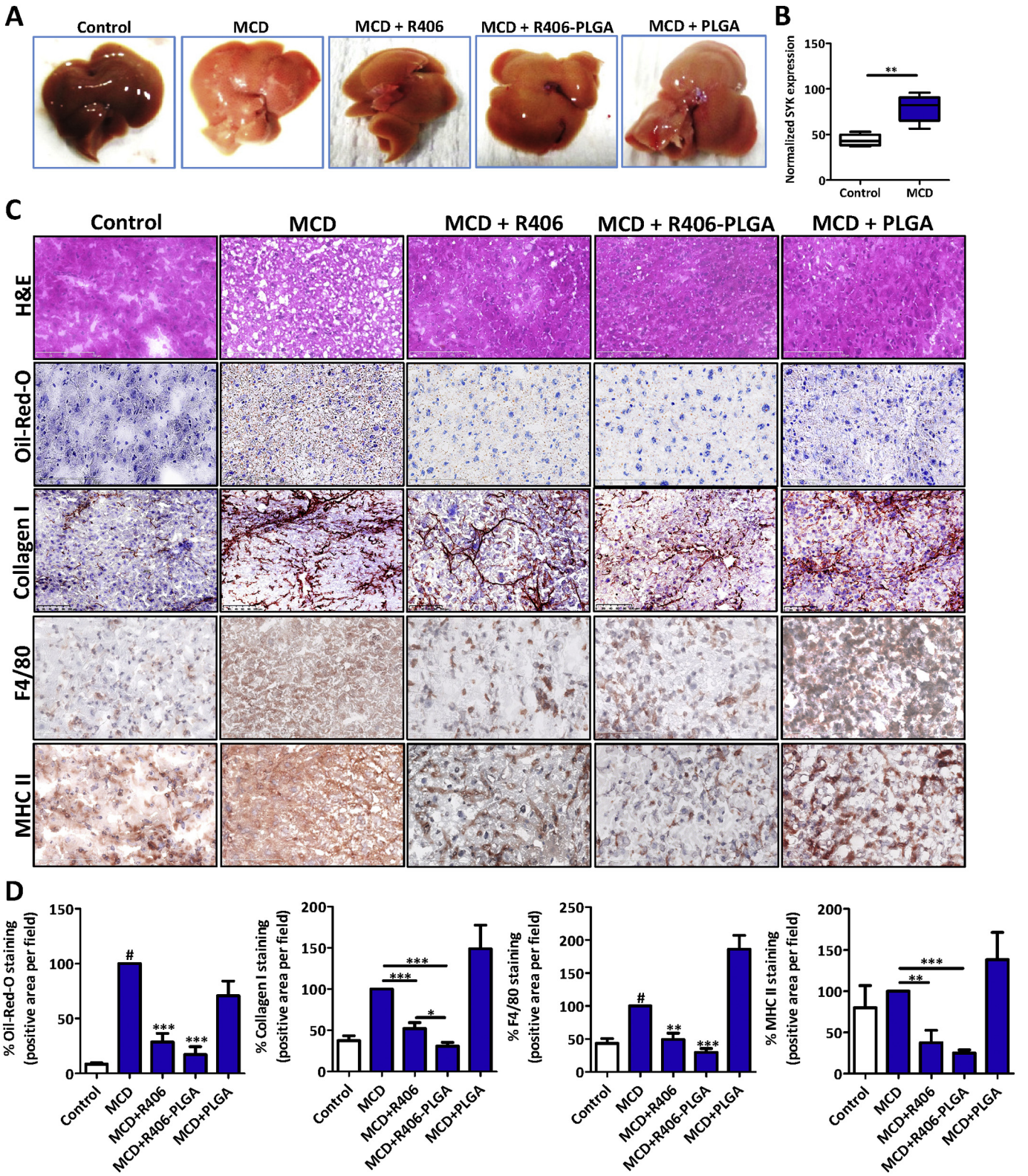

Fig. 7. R406-PLGA ameliorates inflammation, steatosis and fibrosis in methionine and choline-deficient (MCD) diet induced NASH mouse model. (A) Representative images of liver tissue from control group (chow-fed mice, $n = 4$), MCD group (MCD diet-fed mice, $n = 5$), MCD + R406 group (MCD diet-fed mice treated with free drug R406, n = 5), MCD + R406-PLGA group (MCD diet-fed mice treated with R406-PLGA nanoparticles, n = 5), and MCD + PLGA group (MCD diet-fed mice treated with empty PLGA nanoparticles, n = 5). (B) Normalized SYK expression in liver tissue from MCD diet NASH mice (n = 5) compared to control mice (n = 5). $^{**}p < .01$ denotes significance. (C) Representative images of liver sections stained with hematoxylin and eosin (H&E) staining, Oil-red-O staining, and Collagen I, F4/80 and MHC II as performed on healthy controls and MCD diet mice treated with respective treatments. (D) Quantitative image analysis of liver sections from healthy controls and MCD diet mice treated with respective treatments stained with Oil-red-O, collagen I, F4/80 and MHC II. Data are presented as mean + SEM. #p < 0.05 denotes significance versus healthy controls; *p < 0.05, **p < 0.01, ***p < 0.001 denotes significance versus MCD diet mice.

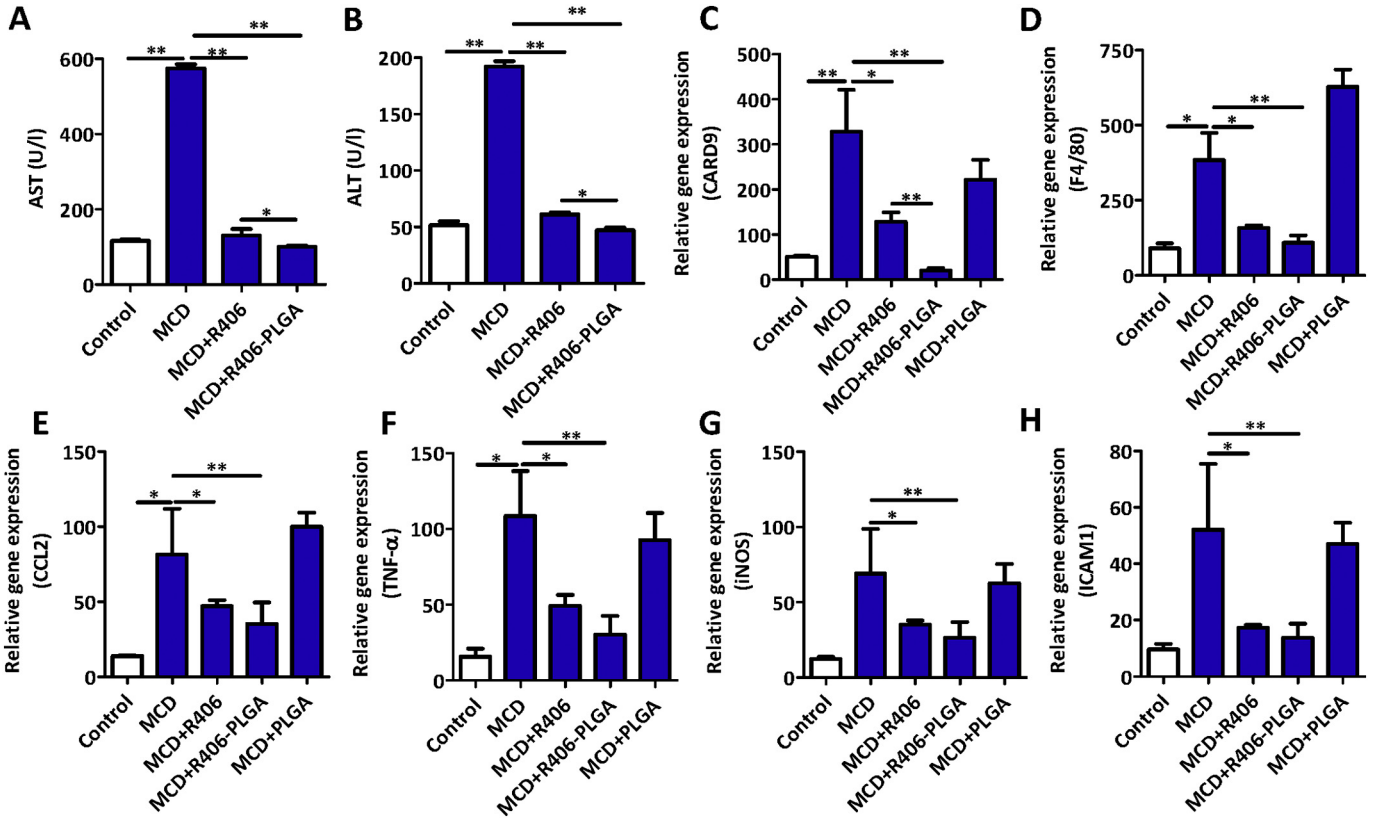

Fig. 8. Increased therapeutic efficacy of R406-PLGA nanoparticles in methionine and choline-deficient (MCD) diet induced NASH in mice. (A) Plasma Aspartate aminotransferase (AST) levels and (B) Plasma Alanine aminotransferase (ALT) levels. Intrahepatic gene expression of (C) CARD9 (caspase recruitment domain-containing 9); (D) macrophage marker F4/80; (E) monocyte chemoattractant protein 1 (MCP1) or chemokine (C—C motif) ligand 2 (CCL2); (F) inflammatory cytokine, tumor necrosis factor alpha (TNF-α); (G) inducible nitric oxide synthase (iNOS or NOS2) and (H) intracellular cell adhesion molecule 1 (ICAM-1). Data are presented as mean + SEM. *p < 0.05, **p < 0.01 denotes significance.

(Fig. 7B). Interestingly, we found that SYK inhibitor R406 and more significantly R406-PLGA nanoparticles ameliorated (a) hepatic inflammation as examined by H&E, F4/80 (macrophage marker) and MHC-II staining's; (b) hepatic fibrosis as confirmed by collagen I (major extracellular matrix protein) expression; and (c) hepatic steatosis as examined using oil-red-o staining (Fig. 7C,D).

We further examined plasma liver transaminases i.e. ALT and AST levels, and found that R406 and more efficiently R406-PLGA inhibited MCD-diet induced AST and ALT levels (Fig. 8A,B). We also analyzed intrahepatic expression of SYK pathway downstream signaling molecule CARD9 (caspase recruitment domain-containing protein 9) [38,39] and found highly significant inhibition of CARD9 by R406-PLGA nanoparticles as compared to R406 (Fig. 8C).

In in vitro studies, we observed that both R406 and R406-PLGA nanoparticles decreased CCL2 (MCP1) expression in RAW macrophages and BMDMs, which was further implicated in the in vivo studies. Reduced intrahepatic CCL2 expression by R406 and R406-PLGA nanoparticles inhibits the macrophage chemotaxis/migration to liver as shown by F4/80 protein expression therefore further inhibiting ongoing liver inflammation (Fig. 7C,D). Previous studies have demonstrated the crucial role of CCL2 in liver inflammation and shown that pharmacological inhibition of CCL2 ameliorated liver inflammation by inhibition of macrophage infiltration [28]. We also analyzed gene expression of F4/80 and crucial inflammatory markers i.e. CCL2, TNFα, iNOS and intracellular cell adhesion molecule 1 (ICAM1), and found that MCD-diet induced the macrophage influx (as shown by F4/80 expression) and inflammatory markers which were inhibited by R406 and more significantly by R406-PLGA nanoparticles suggesting highly beneficial and superior effects of R406-PLGA nanoparticles as compared to R406 alone (Fig. 8D-H).

As previously demonstrated by us, there is a cross-talk between macrophages and hepatic stellate cells (HSCs, major fibrogenic cells in liver) [9,10], therefore reduced inflammation resulted in reduced liver fibrosis as confirmed by collagen I expression. R406 and more strongly, R406-PLGA nanoparticles inhibited collagen I expression (Fig. 7C,D). We further analyzed the gene expression of HSCs specific markers i.e. desmin and alpha smooth muscle actin (α-SMA). We observed that R406 and more potently R406-PLGA nanoparticles significantly inhibited expression of MCD-diet induced HSCs activation while empty PLGA nanoparticles showed no inhibitory effects (Fig. 9A,B). These results collectively suggests that R406-PLGA nanoparticles significantly inhibited fibrosis in MCD-diet induced NASH model.

Finally, we analyzed the effect of R406-PLGA on hepatic steatosis. Oil-Red-O staining showed significant induction in hepatic steatosis in MCD-induced NASH which was inhibited by R406 and more strongly by R406-PLGA nanoparticles (Fig. 7C,D). We first examined total plasma cholesterol and triglyceride levels, and found significant upregulation of these parameters in NASH mice as compared to healthy controls. Interestingly, MCD-diet-induced cholesterol and triglyceride levels were highly significantly inhibited by R406 and, more efficiently, by R406-PLGA nanoparticles (Fig. 9C,D). Furthermore, we analyzed expression of steatosis related markers: UCP1 (uncoupling protein 1), PDRM16 (PR-domain containing 16), PGC1α (Peroxisome proliferator-activator receptor gamma coactivator 1 alpha) and c/EBPβ (CCAAT/enhancing binding protein β). UCP1, PDRM16 and PGC1α has been shown to induce lipid oxidation and hence are involved in PGC1α/PDRM16/UCP1-mediated lipid energy dissipation [39]. c/EBPβ (CCAAT/enhancing binding protein β), has shown to have a key role in steatosis and the pathophysiology of MCD diet-mediated model of NASH through its effect on lipid synthesis, inflammation and ER stress

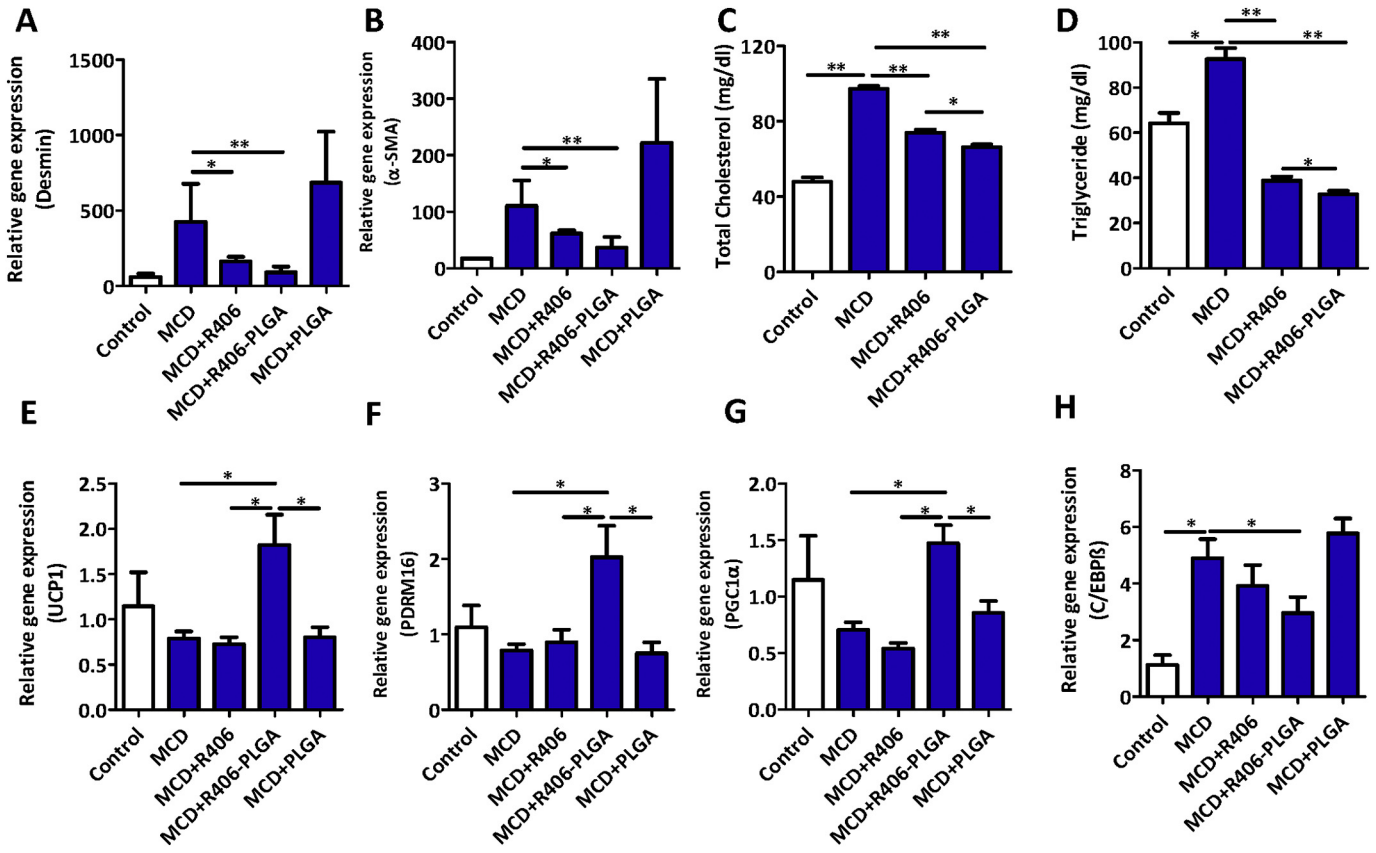

Fig. 9. Increased therapeutic efficacy of R406-PLGA nanoparticles in methionine and choline-deficient (MCD) diet induced NASH in mice. Intrahepatic gene expression of (A) Desmin and (B) α-SMA; (C) Total serum cholesterol levels expressed in mg/dl; (D) Total serum triglyceride levels in mg/dl; Intrahepatic gene expression of (E) uncoupling protein (UCP1); (F) PR domain containing 16 (PDRM16); (G) Peroxisome proliferator-activated receptor gamma coactivator 1-alpha (PGC1α) and (H) c/EBPβ (CCAAT/enhancing binding protein β). Data are presented as mean + SEM. *p < 0.05, **p < 0.01 denotes significance.

[40]. We found that R406-PLGA nanoparticles alone induced the expression of PGC1α, PDRM16, UCP1 and reduced MCD-diet induced C/EBPβ expression suggesting increased lipid oxidation, reduced lipid synthesis and reduced steatosis (Fig. 9E-H). Altogether, these results suggest that R406 and more significantly R406-PLGA nanoparticles significantly ameliorated fibrosis, inflammation and steatosis in NASH mouse model. Importantly, PLGA-mediated delivery significantly increased the in vivo therapeutic efficacy of R406 and therefore potentially reduce the frequency of drug administration.

4. Conclusion

In conclusion, we have demonstrated schematically a novel role of SYK signaling pathway in modulating liver inflammation, fibrosis and steatosis attributed to non-alcoholic steatohepatitis. We have also shown the role of SYK pathway in inflammatory M1 macrophages. Furthermore, this study highlights SYK inhibitor R406 as a potential therapeutic for NASH. Using PLGA nanoparticles, we have demonstrated the efficient intrahepatic delivery of SYK inhibitor for increased therapeutic efficacy as shown by decreased inflammation, hepatic injury, fibrosis and steatosis by suppressing c/EBPβ-mediated lipogenesis and increased PGC1α/PDRM16/UCP1-mediated lipid energy dissipation. To our best knowledge, this is the first study highlighting the increased therapeutic effects of SYK inhibitor using PLGA-mediated delivery in NASH. This promising strategy can potentially be applicable for the treatment of other inflammatory diseases and should be further explored for the systematic evaluation for the clinical applications.

Acknowledgements

This study was funded by Endowment Fund for the Education Republic of Indonesia (Lembaga Pengelola Dana Pendidikan/LPDP RI). This project was partially supported by the Netherlands Organization for Health Research and Development (ZonMW, NWO)-funded VENI innovation grant 916.151.94 (to R.B.). Authors thank Hetty ten Hoopen for her technical assistance.

Appendix A. Supplementary data

Supplementary data to this article can be found online at https://doi.org/10.1016/j.jconrel.2018.09.004.

References

[1] L. Pimpin, H. Cortez-Pinto, F. Negro, E. Corbould, J.V. Lazarus, L. Webber, N. Sheron, Burden of liver disease in Europe: epidemiology and analysis of risk factors to identify prevention policies, J. Hepatol. 69 (2018) 718–735.
[2] S.M. Francque, D. van der Graaff, W.J. Kwanten, Non-alcoholic fatty liver disease and cardiovascular risk: Pathophysiological mechanisms and implications, J. Hepatol. 65 (2016) 425–443.
[3] N. Katsiki, D.P. Mikhailidis, C.S. Mantzoros, Non-alcoholic fatty liver disease and dyslipidemia: an update, Metabolism 65 (2016) 1109–1123.
[4] S.A. Polyzos, C.S. Mantzoros, Nonalcoholic fatty future disease, Metabolism 65 (2016) 1007–1016.
[5] J. Wattacheril, D. Issa, A. Sanyal, Nonalcoholic Steatohepatitis (NASH) and Hepatic Fibrosis: Emerging Therapies, Annu. Rev. Pharmacol. Toxicol. 58 (2018) 649–662.
[6] R. Bataller, D.A. Brenner, Liver fibrosis, J. Clin. Investig. 115 (2005) 209–218.
[7] E. Seki, R.F. Schwabe, Hepatic inflammation and fibrosis: functional links and key pathways, Hepatology 61 (2015) 1066–1079.
[8] R. Bansal, B. Nagorniewicz, J. Prakash, Clinical advancements in the targeted therapies against liver fibrosis, Mediat. Inflamm. 2016 (2016) 7629724.
[9] R. Bansal, J. van Baarlen, G. Storm, J. Prakash, The interplay of the Notch signaling

in hepatic stellate cells and macrophages determines the fate of liver fibrogenesis, Sci. Rep. 5 (2015) 18272.
[10] B. Ozturk Akcora, G. Storm, J. Prakash, R. Bansal, Tyrosine kinase inhibitor BIBF1120 ameliorates inflammation, angiogenesis and fibrosis in CCl4-induced liver fibrogenesis mouse model, Sci. Rep. 7 (2017) 44545.
[11] B.O. Akcora, G. Storm, R. Bansal, Inhibition of canonical WNT signaling pathway by beta-catenin/CBP inhibitor ICG-001 ameliorates liver fibrosis in vivo through suppression of stromal CXCL12, Biochim. Biophys. Acta 1864 (2018) 804–818.
[12] T.N. Bukong, A. Iracheta-Vellve, B. Gyongyosi, A. Ambade, D. Catalano, K. Kodys, G. Szabo, Therapeutic Benefits of Spleen Tyrosine Kinase Inhibitor Administration on Binge Drinking-Induced Alcoholic Liver Injury, Steatosis, and Inflammation in mice, Alcohol. Clin. Exp. Res. 40 (2016) 1524–1530.
[13] T.N. Bukong, A. Iracheta-Vellve, B. Saha, A. Ambade, A. Satishchandran, B. Gyongyosi, P. Lowe, D. Catalano, K. Kodys, G. Szabo, Inhibition of spleen tyrosine kinase activation ameliorates inflammation, cell death, and steatosis in alcoholic liver disease, Hepatology 64 (2016) 1057–1071.
[14] S.H. Shin, K.H. Lee, B.H. Kim, S. Lee, H.S. Lee, J.J. Jang, G.H. Kang, Downregulation of spleen tyrosine kinase in hepatocellular carcinoma by promoter CpG island hypermethylation and its potential role in carcinogenesis, Lab. Investig. 94 (2014) 1396–1405.
[15] C. Qu, D. Zheng, S. Li, Y. Liu, A. Lidofsky, J.A. Holmes, J. Chen, L. He, L. Wei, Y. Liao, H. Yuan, Q. Jin, Z. Lin, Q. Hu, Y. Jiang, M. Tu, X. Chen, W. Li, W. Lin, B.C. Fuchs, R.T. Chung, J. Hong, Tyrosine kinase SYK is a potential therapeutic target for liver fibrosis, Hepatology (2018), https://doi.org/10.1002/hep.29881 (in press).
[16] A. Mocsai, J. Ruland, V.L. Tybulewicz, The SYK tyrosine kinase: a crucial player in diverse biological functions, Nat. Rev. Immunol. 10 (2010) 387–402.
[17] T.N. Bukong, K. Kodys, G. Szabo, Human ezrin-moesin-radixin proteins modulate hepatitis C virus infection, Hepatology 58 (2013) 1569–1579.
[18] T. Oton, L. Silva-Fernandez, J.L. Andreu, Spleen tyrosine kinase (Syk) inhibitor for rheumatoid arthritis, N. Engl. J. Med. 364 (2011) 83.
[19] H. Okamoto, A. Kobayashi, Spleen tyrosine kinase (Syk) inhibitor for rheumatoid arthritis, N. Engl. J. Med. 364 (2011) 83–84.
[20] E.S. Masuda, J. Schmitz, Syk inhibitors as treatment for allergic rhinitis, Pulm. Pharmacol. Ther. 21 (2008) 461–467.
[21] M. Ulanova, F. Duta, L. Puttagunta, A.D. Schreiber, A.D. Befus, Spleen tyrosine kinase (Syk) as a novel target for allergic asthma and rhinitis, Expert Opin. Ther. Targets 9 (2005) 901–921.
[22] K.H. Chen, H.H. Hsu, H.Y. Yang, Y.C. Tian, Y.C. Ko, C.W. Yang, C.C. Hung, Inhibition of spleen tyrosine kinase (syk) suppresses renal fibrosis through anti-inflammatory effects and down regulation of the MAPK-p38 pathway, Int. J. Biochem. Cell Biol. 74 (2016) 135–144.
[23] Y. Kulathu, G. Grothe, M. Reth, Autoinhibition and adapter function of Syk, Immunol. Rev. 232 (2009) 286–299.
[24] M. Bartneck, K.T. Warzecha, F. Tacke, Therapeutic targeting of liver inflammation and fibrosis by nanomedicine, Hepatobiliary Surg Nutr 3 (2014) 364–376.
[25] H.K. Makadia, S.J. Siegel, Poly lactic-co-glycolic acid (PLGA) as biodegradable controlled dDrug delivery carrier, Polymers (Basel) 3 (2011) 1377–1397.
[26] M. Mir, N. Ahmed, A.U. Rehman, Recent applications of PLGA based nanostructures in drug delivery, Colloids Surf B Biointerfaces 159 (2017) 217–231.
[27] G. Sahay, D.Y. Alakhova, A.V. Kabanov, Endocytosis of nanomedicines, J. Control. Release 145 (2010) 182–195.
[28] C. Baeck, X. Wei, M. Bartneck, V. Fech, F. Heymann, N. Gassler, K. Hittatiya, D. Eulberg, T. Luedde, C. Trautwein, F. Tacke, Pharmacological inhibition of the chemokine C-C motif chemokine ligand 2 (monocyte chemoattractant protein 1) accelerates liver fibrosis regression by suppressing Ly-6C(+) macrophage infiltration in mice, Hepatology 59 (2014) 1060–1072.
[29] D.L. Priwitaningrum, J.G. Blonde, A. Sridhar, J. van Baarlen, W.E. Hennink, G. Storm, S. Le Gac, J. Prakash, Tumor stroma-containing 3D spheroid arrays: a tool to study nanoparticle penetration, J. Control. Release 244 ((2016) 257–268.
[30] R. Bansal, J. Prakash, E. Post, L. Beljaars, D. Schuppan, K. Poelstra, Novel engineered targeted interferon-gamma blocks hepatic fibrogenesis in mice, Hepatology 54 (2011) 586–596.
[31] Y.H. Lee, S.H. Kim, S.N. Kim, H.J. Kwon, J.D. Kim, J.Y. Oh, Y.S. Jung, Sex-specific metabolic interactions between liver and adipose tissue in MCD diet-induced nonalcoholic fatty liver disease, Oncotarget 7 (2016) 46959–46971.
[32] M. Ahrens, O. Ammerpohl, W. von Schonfels, J. Kolarova, S. Bens, T. Itzel, A. Teufel, A. Herrmann, M. Brosch, H. Hinrichsen, W. Erhart, J. Egberts, B. Sipos, S. Schreiber, R. Hasler, F. Stickel, T. Becker, M. Krawczak, C. Rocken, R. Siebert, C. Schafmayer, J. Hampe, DNA methylation analysis in nonalcoholic fatty liver disease suggests distinct disease-specific and remodeling signatures after bariatric surgery, Cell Metab. 18 (2013) 296–302.
[33] F. Tacke, Targeting hepatic macrophages to treat liver diseases, J. Hepatol. 66 (2017) 1300–1312.
[34] Y.I. Miller, S.H. Choi, P. Wiesner, Y.S. Bae, The SYK side of TLR4: signalling mechanisms in response to LPS and minimally oxidized LDL, Br. J. Pharmacol. 167 (2012) 990–999.
[35] O. Gross, H. Poeck, M. Bscheider, C. Dostert, N. Hannesschlager, S. Endres, G. Hartmann, A. Tardivel, E. Schweighoffer, V. Tybulewicz, A. Mocsai, J. Tschopp, J. Ruland, Syk kinase signalling couples to the Nlrp3 inflammasome for anti-fungal host defence, Nature 459 (2009) 433–436.
[36] M. Herbrink, B. Nuijen, J.H. Schellens, J.H. Beijnen, Variability in bioavailability of small molecular tyrosine kinase inhibitors, Cancer Treat. Rev. 41 (2015) 412–422.
[37] S.J. Siegel, J.B. Kahn, K. Metzger, K.I. Winey, K. Werner, N. Dan, Effect of drug type on the degradation rate of PLGA matrices, Eur. J. Pharm. Biopharm. 64 (2006) 287–293.
[38] R.A. Drummond, S. Saijo, Y. Iwakura, G.D. Brown, The role of Syk/CARD9 coupled C-type lectins in antifungal immunity, Eur. J. Immunol. 41 (2011) 276–281.
[39] Z. Zhang, L. He, S. Hu, Y. Wang, Q. Lai, P. Yang, Q. Yu, S. Zhang, F. Xiong, S. Simsekyilmaz, Q. Ning, J. Li, D. Zhang, H. Zhang, X. Xiang, Z. Zhou, H. Sun, C.Y. Wang, AAL exacerbates pro-inflammatory response in macrophages by regulating Mincle/Syk/Card9 signaling along with the Nlrp3 inflammasome assembly, Am. J. Transl. Res. 7 (2015) 1812–1825.
[40] S.M. Rahman, J.M. Schroeder-Gloeckler, R.C. Janssen, H. Jiang, I. Qadri, K.N. Maclean, J.E. Friedman, CCAAT/enhancing binding protein beta deletion in mice attenuates inflammation, endoplasmic reticulum stress, and lipid accumulation in diet-induced nonalcoholic steatohepatitis, Hepatology 45 (2007) 1108–1117.